Development 138, 3421-3430 (2011) doi:10.1242/dev.068601

The regenerative capacity of zebrafish reverses cardiac failure caused by genetic cardiomyocyte depletion

Jinhu Wang[1], Daniela Panáková[2], Kazu Kikuchi[1], Jennifer E. Holdway[1], Matthew Gemberling[1], James S. Burris[1], Sumeet Pal Singh[1], Amy L. Dickson[1], Yi-Fan Lin[3], M. Khaled Sabeh[2], Andreas A. Werdich[2], Deborah Yelon[3], Calum A. MacRae[2] and Kenneth D. Poss[1,*]

SUMMARY

Natural models of heart regeneration in lower vertebrates such as zebrafish are based on invasive surgeries causing mechanical injuries that are limited in size. Here, we created a genetic cell ablation model in zebrafish that facilitates inducible destruction of a high percentage of cardiomyocytes. Cell-specific depletion of over 60% of the ventricular myocardium triggered signs of cardiac failure that were not observed after partial ventricular resection, including reduced animal exercise tolerance and sudden death in the setting of stressors. Massive myocardial loss activated robust cellular and molecular responses by endocardial, immune, epicardial and vascular cells. Destroyed cardiomyocytes fully regenerated within several days, restoring cardiac anatomy, physiology and performance. Regenerated muscle originated from spared cardiomyocytes that acquired ultrastructural and electrophysiological characteristics of de-differentiation and underwent vigorous proliferation. Our study indicates that genetic depletion of cardiomyocytes, even at levels so extreme as to elicit signs of cardiac failure, can be reversed by natural regenerative capacity in lower vertebrates such as zebrafish.

KEY WORDS: Cardiomyocyte, Genetic ablation, Heart regeneration, Zebrafish, Epicardium, Endocardium, Heart failure

INTRODUCTION

Heart failure is a disabling, costly human condition of insufficient cardiac output, characterized by exercise intolerance, shortness of breath, edema and increased risk of premature death from arrhythmia or contractile failure. Ischemic, and many non-ischemic, cardiomyopathies commonly involve major cardiac muscle loss and fibrosis, and are primary causes of heart failure (Braunwald and Bonow, 2010; McMurray, 2010). Although the injured adult mammalian heart has a very poor capacity to regenerate cardiac muscle, several directed approaches aim to stimulate this capacity as a means to prevent or treat heart failure. These include identification and manipulation of stem or progenitor cells (Beltrami et al., 2003; Laugwitz et al., 2005; Oh et al., 2003; Winter et al., 2007), reprogramming of non-muscle cells such as fibroblasts into cardiomyocytes (Ieda et al., 2010), or factor delivery to stimulate the limited proliferative ability of cardiomyocytes (Bersell et al., 2009). Although these approaches are promising, they do not yet achieve sufficient cardiac muscle regeneration that would restore function to a failing heart.

Examples of successful heart regeneration exist among vertebrates, and their underlying cellular and molecular mechanisms have the potential to inform future therapies. Cardiac regeneration appears to be an evolutionarily conserved response among adult non-mammalian vertebrate species (Flink, 2002; Kikuchi et al., 2011; Laube et al., 2006; Oberpriller and Oberpriller, 1974; Poss et al., 2002; Rumyantsev, 1973), and regenerative capacity was recently demonstrated in growing hearts of fetal and neonatal mice (Drenckhahn et al., 2008; Porrello et al., 2011). Adult zebrafish are particularly well-studied for their ability to fully regenerate cardiac muscle after surgical resection of ~20% of the ventricle, at or near the maximum amount that can be removed without exsanguination (Poss et al., 2002). Zebrafish hearts also regenerate well after surgery and direct cryoinjury to the ventricle (Chablais et al., 2011; Gonzalez-Rosa et al., 2011; Schnabel et al., 2011). An important mechanistic feature of zebrafish heart regeneration was revealed by recent genetic fate-mapping experiments, which indicated that existing cardiomyocytes are the major source of new muscle after resection of the ventricular apex. Regenerating cardiomyocytes at the injury site display reduced sarcomeric organization, consistent with a mechanism involving some degree of de-differentiation (Jopling et al., 2010; Kikuchi et al., 2010).

Mechanical injury models are not only more tedious and imprecise than desirable, but are limited in their ability to address certain important questions about cardiac regenerative capacity. For example, it is unclear whether larger injuries that might cause signs of acute cardiac failure are subject to similar regenerative capacity and/or mechanisms. Additionally, it is unknown whether internally isolated areas of destroyed myocardium can be effectively replaced with new cardiomyocytes in an adult animal. Finally, whereas mechanical injury removes or destroys many different cardiac cell types and leads to clot formation, cardiac cell type-specific injury models are preferred for certain mechanistic questions; for example, whether cardiomyocyte death on its own, without tissue disruption and clotting, can signal for regeneration. Thus, investigations into new cardiac injury models and potential regenerative responses are crucial for the field.

Here, to address key outstanding issues, we generated a transgenic system to inflict extreme myocardial injury of much greater specificity and severity than has been achieved in previous

[1]Department of Cell Biology and Howard Hughes Medical Institute, Duke University Medical Center, Durham, NC 27710, USA. [2]Cardiovascular Division, Brigham and Women's Hospital, Harvard Medical School, Boston, MA 02115, USA. [3]Division of Biological Sciences, University of California-San Diego, La Jolla, CA 92093, USA.

*Author for correspondence (kenneth.poss@duke.edu)

Accepted 9 June 2011

studies. Injuries achieving destruction of >60% of the ventricular myocardium disrupted electric conduction and elicited signs of severe cardiac failure. Yet, an injury response involving all major cardiac cell types was stimulated that rapidly replaced lost myocardium and ameliorated symptoms. This regenerative process featured widespread proliferation by a high percentage of spared cardiomyocytes, cells that displayed multiple indicators of de-differentiation. Our findings demonstrate that adult zebrafish possess a striking capacity for activating regeneration from spared cardiomyocytes after genetically induced muscle loss.

MATERIALS AND METHODS

Zebrafish and heart injuries

Outbred EK or EK/AB mixed background zebrafish (4-10 months of age) were used for ventricular resection surgeries as described previously (Poss et al., 2002), or for cardiomyocyte ablation. Animal density was maintained at approximately four fish per liter in all experiments. To ablate cardiomyocytes, anesthetized Z-CAT fish were injected intraperitoneally with 0.5 mg/ml 4-hydroxytamoxifen (4-HT) in 10% ethanol as described previously (Kikuchi et al., 2010). For bath treatment, animals were treated for 12 hours in 0.02 μM, 0.1 μM or 0.5 μM 4-HT in fish water. Other transgenic strains used were: *cmlc2:actinin3-EGFP* (Y.-F.L. and D.Y., unpublished), *fli1:EGFP* (Lawson and Weinstein, 2002) and *bactin2:loxp-DsRed-STOP-loxp-EGFP* (Kikuchi et al., 2010). Newly constructed strains are described in the section below. All transgenic strains were analyzed as hemizygotes. All animal procedures were performed in accordance with Duke University guidelines.

Heat stress experiments

Animals with resection injuries, or Z-CAT fish injected with 0.5 mg/ml 4-HT or 10% vehicle, were exposed at 7 days post-injection (dpi) to a transient, automated increase in temperature from 26°C to 38°C, as described (Lee et al., 2005). With this protocol, animals remained at 38°C for one hour before gradual return to 26°C.

Maximum swimming speed and endurance experiments

To evaluate swimming performance, male animals with resection injuries, or male Z-CAT fish that had been treated previously with 0.1 μM 4-HT or vehicle for 12 hours, were placed in a swim tunnel respirometer (Mini Swim-170, Loligo Systems, Denmark) and allowed to acclimatize for 20 minutes at a low flow velocity of 3 cm/s. Swimming speed was then increased in stages of 3-6 cm/s every 2 minutes. There were six to nine stages following the acclimation period during which velocity was increased, with the final stage having a velocity of 26 cm/s in 7 dpi tests and 37 cm/s at 14 and 30 dpi. Once fish showed exhaustion and were unable to release from the downstream screen of the swim chamber, the time and stage were recorded. Tests ended at 32 minutes, with several vehicle-injected animals successfully reaching the endpoint. For swimming endurance, the velocity was increased to 20 cm/s following the acclimatization period and kept constant, and the time until exhaustion was recorded.

Histological methods

In situ hybridization (ISH) on 10 μm cryosections of paraformaldehyde-fixed hearts was performed using digoxygenin-labeled cRNA probes as described (Poss et al., 2002) with the aid of an InSituPro robot (Intavis). Acid Fuchsin-Orange G staining was performed as described (Poss et al., 2002). Primary antibodies used in this study were: anti-Mef2 (rabbit; Santa Cruz Biotechnology), anti-Myosin heavy chain (MHC; F59, mouse; Developmental Studies Hybridoma Bank), anti-GFP (rabbit; Invitrogen), anti-DsRed (rabbit; Clontech), anti-BrdU (rat; AbD) and anti-PCNA (mouse; Sigma). Secondary antibodies (Invitrogen) used in this study were: Alexa Fluor 488 goat anti-rabbit; Alexa Fluor 594 goat anti-rabbit, goat anti-rat and goat anti-mouse; and Alexa 633 goat anti-mouse. Myeloperoxidase staining was performed using a kit from Sigma-Aldrich (390A-1KT) following manufacturer's instructions. FITC-labeled phalloidin was obtained from Sigma. Immunofluorescence and terminal deoxynucleotidyl transferase dUTP nick end labeling (TUNEL) staining on cryosections were performed as described (Kikuchi et al., 2011).

Myofiber area was measured by imaging three medial, longitudinal F59-stained ventricular sections for each animal, quantifying the fluorescent and total ventricular areas using Openlab and ImageJ software, and calculating an average number of fluorescent pixels per mm^2 of ventricular tissue. To calculate cardiomyocyte proliferation indices, ventricular (or atrial) sections were stained with antibodies against Mef2 and PCNA. For ablation injuries, three medial, longitudinal sections of each ventricle were selected for analysis, and high-magnification images were taken of different ventricular regions and merged using Photoshop software to represent the entire ventricular section. $Mef2^+$ and $Mef2^+PCNA^+$ cells were counted manually with the aid of ImageJ software, with 400-3000 cardiomyocytes assessed per animal. For resection injuries, we imaged the three ventricular sections with the largest injuries, and quantified $Mef2^+$ and $Mef2^+PCNA^+$

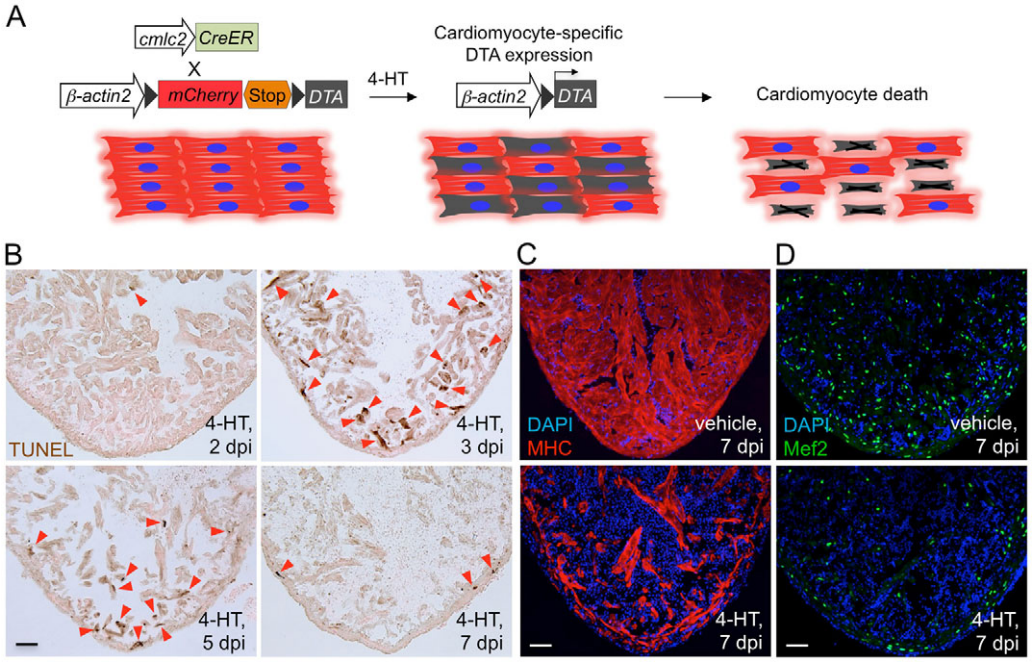

Fig. 1. Genetic ablation of adult zebrafish cardiomyocytes. (**A**) Schematic representation of transgenes used for zebrafish cardiomyocyte ablation. DTA is specifically expressed in cardiomyocytes upon 4-HT treatment. (**B**) TUNEL staining of ventricular muscle from transgenic animals injected with vehicle or 4-HT (0.5 mg/ml). Arrowheads indicate TUNEL-positive cardiac myocytes. (**C**) Myosin heavy chain (MHC) staining of ventricular sections after vehicle or 4-HT injection, shown at 7 days post-injection (dpi). (**D**) Mef2 staining to indicate cardiomyocyte nuclei, showing major cellular losses in 4-HT-injected animals. Scale bars: 50 μm.

cells within a defined region, typically including almost all $Mef2^+PCNA^+$ cells near the injury (216 pixels in vertical). The percentages of $Mef2^+PCNA^+$ cells from the three selected sections were averaged to determine a proliferation index for each animal.

For transmission electron microscopy (TEM), injured hearts were fixed in 2% glutaraldehyde/4% formaldehyde. Tissue was embedded using the EMbed 812 resin kit (with DMP-30) (EMS) and sectioned to 70-90 nm thickness using Ultracut or Ultracut E ultra-microtomes (Leica). Microscopy was performed on a FEI Tecnai G2 Twin (200kv) transmission electron microscope and images were obtained using a FEI Eagle camera.

4-HT labeling and quantification of EGFP fluorescence in Z-CAT; *bactin2:loxp-DsRed-STOP-loxp-EGFP* animals

To quantify Cre-mediated release of EGFP expression in lineage-tracing experiments with Z-CAT; *bactin2:loxp-DsRed-STOP-loxp-EGFP* animals, three medial, longitudinal sections were selected from each heart and stained with F59. Images of single optical slices of the ventricle were taken using a 20× objective (1024×1024 pixels) by adjusting gain to detect EGFP or MHC signals above background level. To obtain an entire single slice image, we merged images of different ventricular regions using Photoshop software. $EGFP^+$ and MHC^+ areas were quantified in pixels by ImageJ software, and the percentage of $EGFP^+MHC^+$ versus MHC^+ area was calculated for each heart.

Optical mapping and data analysis

Detailed methods have been previously described (Kikuchi et al., 2010). Briefly, hearts from anesthetized fish were isolated in Tyrode's solution and stained with 56 μM di-4-ANEPPS (D-1199, Invitrogen) for 10 minutes. For data acquisition, hearts were transferred to Tyrode's solution with 30 μM of blebbistatin (EMD Chemicals) and point stimulated with a fine platinum electrode at the base of the ventricle at 80 beats/minute. Optical action potentials were recorded from the epicardial surface of the ventricle. Acquired fluorescence data were analyzed with custom-written software (MatLab, Mathworks) as previously described (Kikuchi et al., 2010; Panakova et al., 2010) Signals were processed with temporal (200 Hz cutoff) and spatial (4-pixel weighted average) filters. Epicardial surface conduction velocities were estimated from regions of interest (ROIs; 156×156 μm) near the apex of each heart. Action potential durations were estimated as the time interval between 20% depolarization and 80% repolarization (APD_{80}). Derived maximum action potential upstroke velocities were calculated as the maximum of the first time-derivative of the action potential upstroke. The data were processed and analyzed using GraphPad Prism5.

Construction of transgenic animals

bactin2:loxp-mCherry-STOP-loxp-DTA

A cassette containing a floxed mCherry followed by five repeats of polyadenylation (pA) sites was subcloned behind the zebrafish *β-actin2* promoter (Traver et al., 2003). The pA repeats were derived from *sox10-GFP-DTA* (provided by W. Richardson, London, UK) and pBigT (Srinivas et al., 2001). The mutated version of DTA (G383A) (provided by M. Capecchi, Salt Lake City, UT, USA) was amplified by PCR using the following primers: 5′-CCGGATCGATACGCGTCCCTAGCCATGGG-CGCTGATGATGTTGTTGATTCTTCT-3′, and 5′-CCGGCTCGAGTTA-TCATCGCCTGACACGATTTCCTGCACAG-3′, and subcloned behind the floxed mCherry cassette. The entire cassette was flanked with 2× core insulator elements and I-*Sce*I sites, and co-injected with I-*Sce*I into one-cell-stage zebrafish embryos. The full name of this transgenic line is *Tg(bactin2:loxP-mCherry-STOP-loxP-DTA176)*^{pd36}.

tcf21:nucEGFP

The translational start codon of *tcf21* in the BAC clone DKEYP-79F12 was replaced with the *nucEGFP* cassette by Red/ET recombineering technology (GeneBridges). The 5′ and 3′ homologous arms for recombination were a 50-base-pair (bp) fragment upstream of the start codon, and a 50-bp fragment downstream, respectively, and were included in PCR primers to flank the *nucEGFP* cassette. To avoid potential mis-recombination between the *nucEGFP* cassette and an endogenous *loxP* site in the BAC vector, we replaced the vector-derived *loxP* site with an I-*Sce*I site using the same technology. The final BAC was purified with Nucleobond BAC 100 kit (Clontech), and co-injected with I-*Sce*I into one-cell-stage zebrafish embryos. The full name of this transgenic line is *Tg(tcf21:nucEGFP)*^{pd41}.

RESULTS

Genetic ablation of adult zebrafish cardiomyocytes

Modeled on studies using mice (Akazawa et al., 2004; Breitman et al., 1987; Brockschnieder et al., 2004; Lee et al., 1998; Saito et al., 2001; Stanger et al., 2007), we generated a double transgenic system to facilitate cell type-specific ablation in zebrafish. The first transgenic line has a 4-hydroxytamoxifen (4-HT)-inducible Cre recombinase (CreER) restricted to cardiomyocytes by the *cmlc2* (*myl7* – Zebrafish Information Network) promoter, as described recently (*cmlc2:CreER*) (Kikuchi et al., 2010). We created a second line (*bactin2:loxp-mCherry-STOP-loxp-DTA*) that targets cytotoxic DTA (diptheria toxin A chain) expression to *CreER*-expressing cells upon 4-HT injection (Fig. 1A). The β-*actin2* promoter fragment drives expression strongly in myocytes, with little or no expression in epicardium and endocardium (Kikuchi et al., 2010). We intentionally selected a line that displayed moderate mCherry expression in what appeared to be most, if not all, cardiomyocytes (see Fig. S1A in the supplementary material). To test the efficiency of myocyte ablation, we intercrossed these lines and injected 6-month-old *cmlc2:CreER*; *bactin2:loxp-mCherry-STOP-loxp-DTA* animals intraperitoneally with 0.5 mg/ml 4-HT. This treatment was

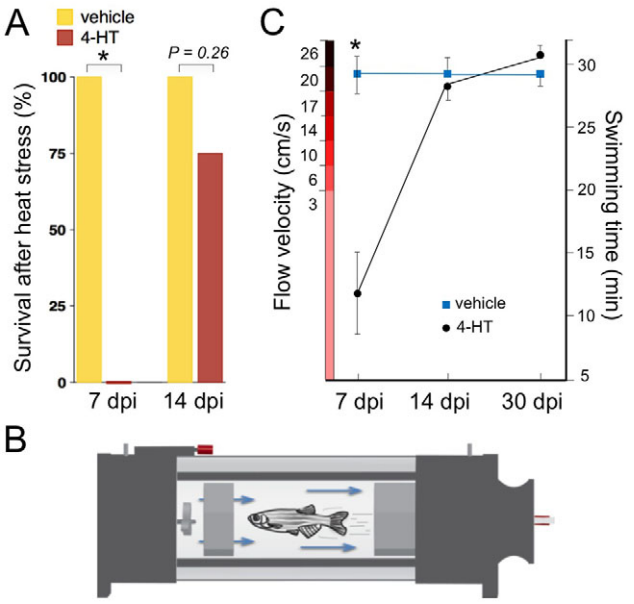

Fig. 2. Stress response and swimming performance after cardiomyocyte ablation. (**A**) Survival of Z-CAT after a strong heat shock is given 7 and 14 days after vehicle or 4-HT injection. For each group, 9-13 zebrafish were assessed. Fisher Irwin exact test, *P<0.05. (**B**) Cartoon representing assay for swimming performance, in which adult zebrafish must swim to maintain position in a controlled current. (**C**) Maximum swimming speed of Z-CAT fish injected with vehicle or 4-HT at 7, 14 and 30 days post-injection (dpi). At each time point, 7-15 animals were assessed. Several vehicle-treated animals maintained swimming orientation throughout the 32-minute test periods; thus, 7 dpi data under-represent differences between the groups. *P<0.05, Student's t-test. Mean±s.e.m.

typically not lethal, and TUNEL-positive ventricular myocytes indicative of apoptosis were initially observed 2 days post-injection (dpi). Myocyte cell death was observed at high frequencies, was distributed diffusely and uniformly throughout the ventricle at 3 and 5 dpi, and diminished by 7 dpi (Fig. 1B).

We used multiple assays to confirm and quantify cardiomyocyte ablation 7 days after a single injection of 0.5 mg/ml 4-HT, which became our standard protocol. Histology and digital quantification of muscle marker expression indicated that 61% of Myosin heavy chain (MHC)-positive or phalloidin-stained myocardium was depleted from ventricular sections (Fig. 1C and Fig. 3B; see Fig. S1B in the supplementary material). Examination of Mef2, a nuclear marker of cardiomyocytes, indicated that this corresponded to depletion of 71% of Mef2^{+} nuclei (Fig. 1D and Fig. 3C). We also induced cardiomyocyte ablation by bath incubation of animals in 4-HT. Treatment with 500 nM 4-HT for 12 hours destroyed more than twice as much ventricular muscle as treatment with 20 nM 4-HT (see Fig. S1B,C in the supplementary material). Multiple injections of 0.5 mg/ml 4-HT were typically lethal within a few days and revealed destruction of 80% or more of the ventricular myocardium by histology (data not shown). Thus, *cmlc2:CreER*; *bactin2:loxp-mCherry-STOP-loxp-DTA* animals facilitate dose-dependent ablation of a large proportion of ventricular cardiomyocytes. For brevity, we refer to this double transgenic system as Z-CAT (zebrafish cardiomyocyte ablation transgenes).

Rapid regeneration after cardiomyocyte ablation and indicators of cardiac failure

Rodents typically exhibit heart failure after destruction of 40-50% of left ventricular cardiomyocytes by coronary artery occlusion, whereas 30% myocardial loss is fatal to dogs (Pfeffer et al., 1979). Loss of 20-30% of human ventricular myocytes has been associated with end-stage cardiomyopathy requiring cardiac transplantation (Beltrami et al., 1994). Interestingly, diffuse, DTA-mediated ablation of just 10-20% of murine myocytes was recently reported to cause heart failure (Akazawa et al., 2004). Observation of 4-HT-injected (0.5 mg/ml) Z-CAT animals at rest indicated marked lethargy typically from 6 dpi to ~10 dpi, as well as a rapid gasping/breathing phenotype (see Movies 1 and 2 in the supplementary material). To test for additional possible signs of cardiac failure, we subjected injured Z-CAT animals to stress and exercise regimens. First, we gave them a single 38°C heat-shock 7 days after 4-HT injection. Whereas vehicle-injected Z-CAT animals survived normally, all animals injected with 4-HT died during the heat-shock, indicating severe stress hypersensitivity (Fig. 2A). We next tested exertion capacity by placing animals in a swim tube with a tunable water flow velocity (Fig. 2B). Whereas vehicle-injected Z-CAT animals performed well with increasing flow velocity, those injected with 4-HT unsuccessfully maintained orientation against these currents at 7 dpi, indicating reduced exercise tolerance (Fig. 2C; see Movies 3 and 4 in the supplementary material). We assessed whether zebrafish displayed any of these phenotypes 3-4 days after surgical resection of 20% of the ventricle, a time chosen to allow sufficient recovery from invasive surgery but prior to detectable muscle regeneration. Importantly, lethargic appearance, gasping phenotypes and reduced stress sensitivity were not seen in these animals, and their swimming performance was not significantly different from uninjured animals (see Fig. S2; Movies 5 and 6 in the supplementary material). These assays indicated that the Z-CAT injury model was unique in eliciting signs of cardiac failure, confirming our histological assessment of considerably more severe muscle loss than after surgical resection.

To test for recovery, we performed the same assays in Z-CAT animals at 14 dpi. Strikingly, lethargy and gasping phenotypes were much less common at this stage, with full recovery in the majority of animals who had shown these phenotypes at 7 dpi (see Movie 7 in the supplementary material). Similarly, a strong heat-shock was lethal to just 25% of 4-HT-injected Z-CAT animals, indicating an improvement in stress resistance (Fig. 2A). Finally, by testing

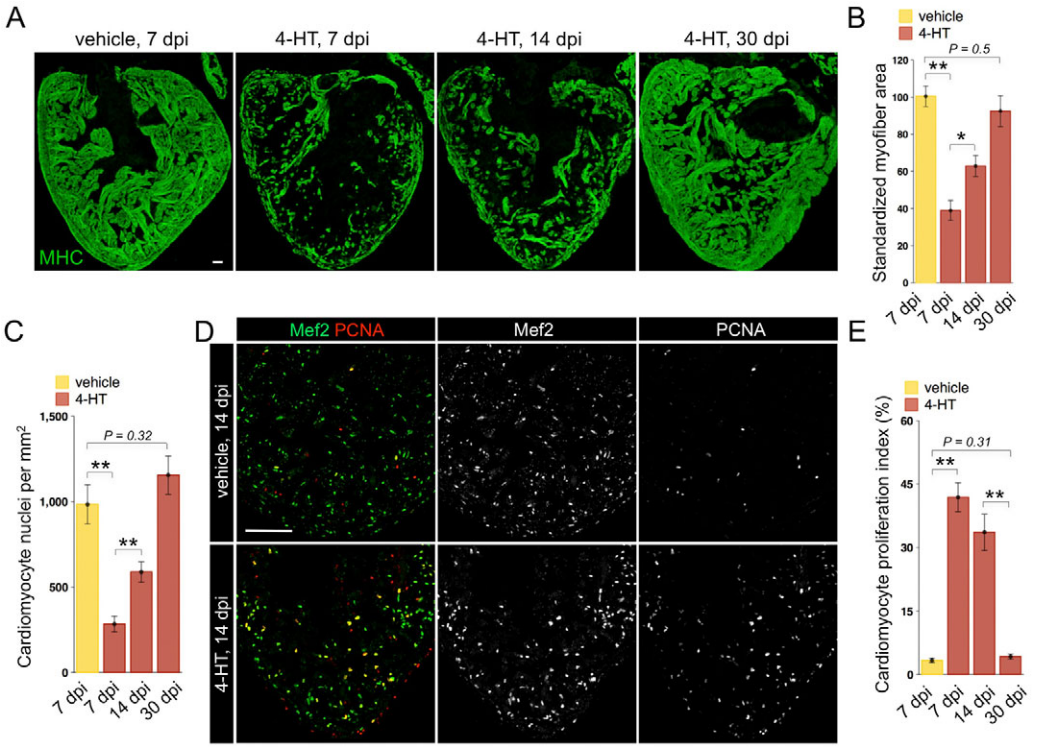

Fig. 3. Rapid regeneration of ventricular cardiomyocytes after ablation-induced injuries. (**A**) Myosin heavy chain (MHC) staining of ventricular sections from Z-CAT fish injected with vehicle or 4-HT, at 7, 14 and 30 days post-injection (dpi). For each group, 5-7 animals were assessed. (**B**) Quantification of MHC^{+} myofiber area from experiments in A. (**C**) Quantification of Mef2^{+} cardiomyocyte nuclei from experiments in A. (**D**) Ventricular cardiomyocyte proliferation at 14 dpi assessed by Mef2 and PCNA staining. 4-HT-injected animals display widespread PCNA^{+} cardiomyocytes. (**E**) Quantification of ventricular cardiomyocyte proliferation in Z-CAT animals injected with vehicle or 4-HT, at 7, 14 and 30 dpi. For each group, seven to nine animals were assessed. *P<0.05, **P<0.005, Student's t-test. Mean±s.e.m. Scale bars: 50 μm.

exercise tolerance in the same animals that had underperformed at 7 dpi, we found substantial improvements to the levels of control animals (Fig. 2C). Swimming endurance, the average time during which animals could maintain orientation in a high velocity current, was not different in vehicle- and 4-HT-injected animals at 45 dpi (data not shown). Thus, massive ablation of ventricular muscle dramatically reduced the performance of adult zebrafish during stress and exercise, but these abilities recovered within several days.

We next assessed histological evidence that might explain this recovery. Quantifications of myofiber area and Mef2^{+} cardiomyocyte nuclei at 14 dpi indicated that animals restored 39% of lost myofiber area (to 63% of that of vehicle-treated animals) and 44% of lost myocyte nuclei (to 60%) within one week. These measurements suggested that zebrafish require between ~40 and 60% of their cardiomyocytes for normal performance in the exercise assay that we used. By 30 dpi, ventricles were fully muscularized (Fig. 3A-C). Measurements of ventricular section surface area at 30 dpi indicated no increases in cardiac size with this nuclear recovery (see Fig. S1E in the supplementary material), suggesting that cellular hypertrophy is not a major component of muscle restoration. To determine whether muscle restoration occurred as a result of cell proliferation, we assessed the percentage of myocytes expressing the marker proliferating cell nuclear antigen (PCNA), which compares well with BrdU incorporation assays (see Fig. S3 in the supplementary material) (Wills et al., 2008). Whereas 3% of myocytes were PCNA^{+} in vehicle-treated Z-CAT animals, 42% of myocytes displayed nuclear PCNA at 7 days after 4-HT injection, and 34% at 14 dpi. These proliferating cardiomyocytes were distributed throughout the ventricle, suggesting that most cardiomyocytes can participate in the regenerative response. Cardiomyocyte proliferation returned to near baseline levels by 30 dpi, concomitant with muscularization (Fig. 3D,E). We also confirmed that scarring, the predominant response of mammals to cardiac injury, was not a significant response to myocardial ablation. Slight increases in cardiac collagen deposition were occasionally observed at 14 dpi and 30 dpi compared with control animals. However, large deposits were generally not detected, even at 180 dpi (see Fig. S4 in the supplementary material; data not shown). Our data indicate rapid and complete regeneration after ablation-induced muscle damage that was severe enough to elicit signs of cardiac failure.

Robust injury responses by ventricular non-muscle cells and atrial myocytes after genetic cardiomyocyte ablation

Prior to this study, it had not been known whether diffuse, extensive adult cardiomyocyte loss could be replaced through regeneration. In addressing this, our results indicated considerably more efficient regeneration in this context than from the injury zone cardiomyocytes that are spared by resection of the zebrafish ventricle. In that case, regeneration is typically completed by 1-2

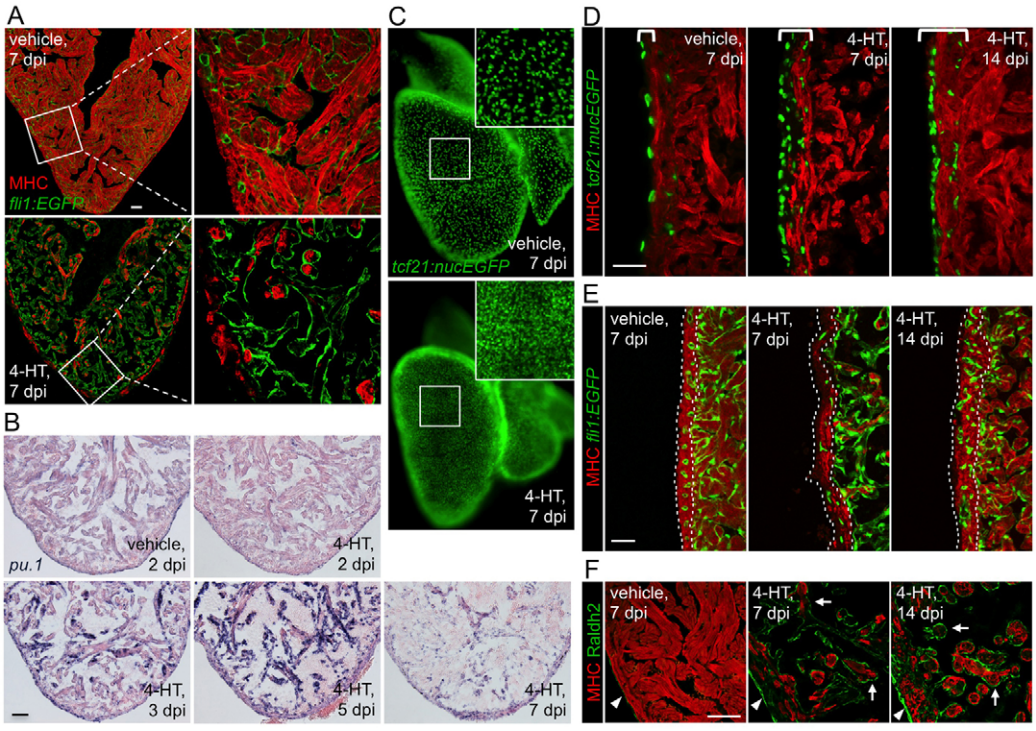

Fig. 4. Effects of cardiomyocyte ablation on non-muscle cells. (**A**) Visualization of endocardial cells (green) and muscle (red) in sections from vehicle-or 4-HT-injected Z-CAT fish. The endocardial layer appears intact one week after massive cardiomyocyte loss. Single confocal slices are shown. (**B**) In situ hybridization for *pu.1*-expressing cells, which are prominent by 3-5 dpi. (**C**) Whole-mount visualization of epicardial nuclei in vehicle- or 4-HT-injected Z-CAT fish at 7 dpi, indicating higher epicardial cell density after myocardial injury. Inset shows enlarged view of boxed area. (**D**) Histological visualization of epicardial cells after myocardial ablation. Epicardial cells proliferate by 7 dpi and are incorporated into the regenerating myocardial wall by 14 dpi. Brackets indicate area containing *tcf21*-expressing epicardial cells. (**E**) Visualization of coronary vascular endothelial cells (green) in sections of the ventricular wall (outlined by dotted lines). Coronary vasculature is reduced in 4-HT-injected Z-CAT animals by 7 dpi, but restored by 14 dpi. (**F**) Sections from Z-CAT ventricles stained for the retinoic acid (RA)-synthesizing enzyme Raldh2. RA synthesis appears low in vehicle-injected tissue, but is strongly induced in epicardial (arrowheads) and endocardial (arrows) structures after cardiomyocyte ablation. Single confocal slices are shown. Scale bars: 50 μm.

months post-injury, with only 10-15% of cardiomyocytes at the resection plane proliferating (PCNA$^+$) at 7 dpa (Kikuchi et al., 2011; Poss et al., 2002). Interestingly, in mammalian skeletal muscle, regeneration is poor when large areas of muscle and connective tissue are removed, e.g. by amputation; yet, injuries that preserve the connective tissue scaffolding permit vigorous regeneration (Tajbakhsh, 2009). Thus, we surmised that the presence and activity of analogous, non-muscle components like endocardial, epicardial and vascular cells contribute to regenerative efficacy after cardiomyocyte ablation.

To visualize endocardial cells that line the inner, trabecular myocardium, we crossed the *fli1:EGFP* transgene into the Z-CAT background. We found that endocardial architecture was grossly intact at 7 dpi despite cardiomyocyte depletion (Fig. 4A). We examined injured ventricles for macrophage presence within and around these endocardial structures. In situ hybridization with a *pu.1* (*spi1* – Zebrafish Information Network) probe showed little staining in vehicle-treated Z-CAT vehicles. By contrast, upon cardiomyocyte ablation there was a massive enrichment of injured trabecular myofibers as well as the compact myocardial layer with *pu.1*$^+$ cells, most prominently at 3 and 5 dpi, periods of peak cell death (Fig. 4B). This inflammatory response to cardiomyocyte ablation also included neutrophil recruitment, as assessed by myeloperoxidase staining (see Fig. S5 in the supplementary material). Thus, the endocardium is spared after severe myocyte ablation, and endocardial-coated pockets of ablated myocardium are targets of macrophage and neutrophil infiltration.

The peripheral compact muscle is surrounded and penetrated by epicardial cells rather than endocardium. To visualize epicardium, we generated a new transgenic strain reporting nuclear-localized EGFP in virtually all epicardial cells (*tcf21:nucEGFP*). Epicardial cells surrounding the ventricle were stimulated by ablation injury to proliferate and form a multilayered structure by 7 dpi (Fig. 4C,D). By 14 dpi, these augmented epicardial cells became incorporated into the underlying myocardial wall, events suggestive of epithelial-mesenchymal transition (Fig. 4D). The epicardium has been proposed to support neovascularization during regeneration, analogous to its known embryonic roles (Kim et al., 2010; Lepilina et al., 2006; Kikuchi et al., 2011). We observed an initial reduction in the density of vessels within the ventricular wall at 7 dpi. However, one week later and concomitant with muscle regeneration, the ventricular wall was well-vascularized, indicative of a neovascularization process (Fig. 4E).

Endocardial and epicardial cells are likely to impact cardiac muscle regeneration in several ways. Soon after resection injury, retinoic acid (RA) synthesis, as visualized by expression of the enzyme Raldh2 (Aldh1a2 – Zebrafish Information Network), is increased in endocardial and epicardial cells throughout the injured ventricle and uninjured atrium (Kikuchi et al., 2011; Lepilina et al., 2006; Wills et al., 2008). During regeneration, RA production localizes to injuries, where RA signaling is essential for cardiomyocyte proliferation (Kikuchi et al., 2011). Raldh2 was induced and maintained strongly and throughout ventricular endocardial and epicardial tissue at 7 and 14 days, adjacent to regions of ablated myocardium (Fig. 4F). We expect that this response to ablation injury is likely to have the same function as after resection injury. In total, these analyses indicate that widespread cardiomyocyte-specific cell ablation elicits strong injury responses from non-myocardial cells, including endocardial and epicardial RA production, epicardial proliferation and neovascularization, all of which are likely to impact rapid regeneration from extreme cardiac damage.

Finally, we also took advantage of this ablation system to assess atrial myocyte regeneration. The zebrafish atrium is difficult to access surgically, and its regenerative capacity has not previously been assessed. Because atrial muscle is also subject to genetic

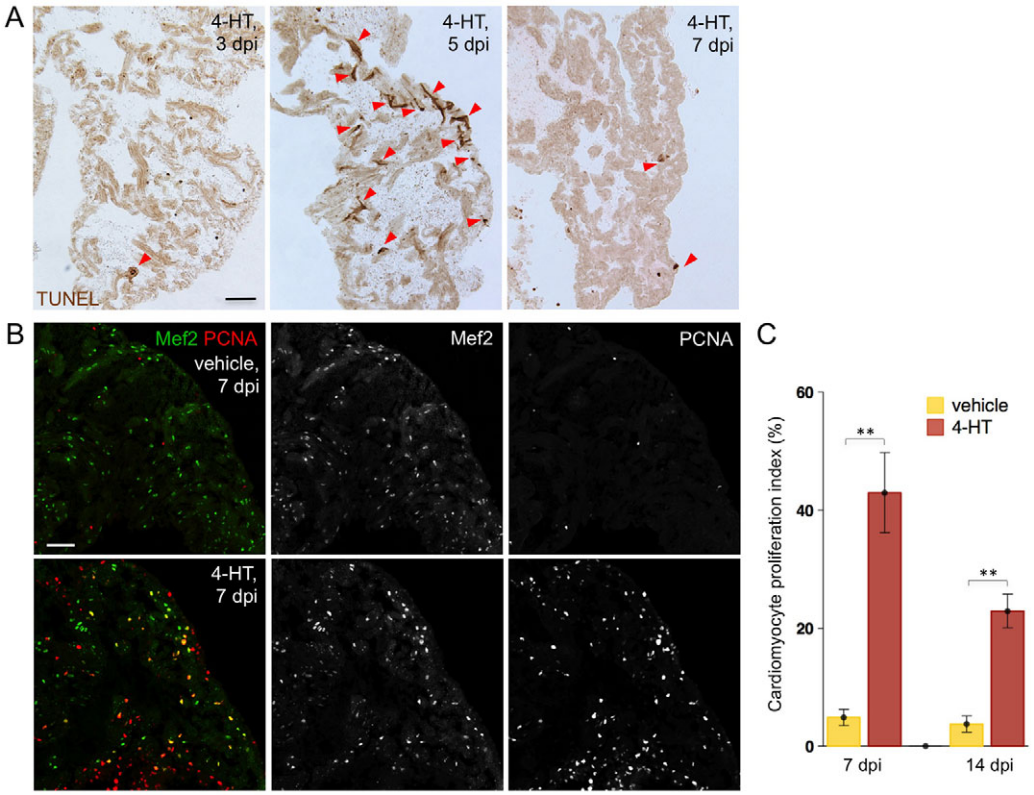

Fig. 5. Atrial cardiomyocyte ablation and regeneration. (**A**) TUNEL staining of atrial sections from Z-CAT fish injected with 4-HT. Arrowheads indicate TUNEL-positive muscle. (**B**) Cardiomyocyte proliferation at 7 days post-injection (dpi) in atrial sections from Z-CAT animals injected with vehicle or 4-HT, assessed by Mef2 and PCNA staining. 4-HT-injected animals display widespread atrial PCNA$^+$ cardiomyocytes. Scale bars: 50 μm. (**C**) Quantification of atrial cardiomyocyte proliferation in Z-CAT fish injected with vehicle or 4-HT, at 7 and 14 dpi. For each group, six to eight animals were assessed. Mean±s.e.m. $^{**}P<0.005$, Student's *t*-test.

ablation via the *cmlc2* promoter, we examined apoptosis and proliferation in this chamber after an injection of 0.5 mg/ml 4-HT. Atrial myocyte apoptosis showed similar dynamics as ventricular myocytes, with evenly distributed TUNEL-positive myocytes by 5 dpi (Fig. 5A). Atrial myocyte proliferation indices were 43% at 7 days and 23% at 14 dpi, versus 4% in vehicle-injected Z-CAT fish, indicative of a strong regenerative response (Fig. 5B,C). Thus, the zebrafish atrium, like the ventricle, is highly regenerative after major ablation injury.

Ultrastructural and physiological de-differentiation in source myocytes during regeneration

To determine the source of new cardiomyocytes regenerated after ablation injury, we crossed a lineage-tracing reporter transgene (*bactin2:loxp-DsRed-STOP-loxp-EGFP*) into Z-CAT. Recombination between *loxp* sites releasing EGFP expression is more efficient than events releasing DTA expression, and resulted in 96% of spared ventricular muscle being labeled with EGFP at 7 dpi after myocardial ablation (Fig. 6A-C). Assessment of ventricles at 30 dpi indicated that, similarly, 95% of regenerated muscle retained the EGFP label (Fig. 6B,C). To determine whether cardiomyocytes dissembled sarcomeres during ablation-induced regeneration, we crossed a Z-line-labeling *cmlc2:actinin3-EGFP* transgene into Z-CAT. At 7 dpi, and more so at 14 dpi, there were many cardiomyocytes with visibly disordered sarcomere structure, a phenotype indicative of a more primitive differentiation state and reduced contractile properties (Fig. 6D). These observations were corroborated by transmission electron microscopy, which also revealed disorganized myocyte sarcomere structure at 7 and 14 dpi (Fig. 6E). Sarcomere disorganization was coincident with cardiomyocyte proliferation and subsequent to cardiomyocyte apoptoses, making it unlikely that they reflect dying DTA-expressing cells. Also, the sudden appearance of disorganized sarcomeres in a high percentage of myocardium throughout the ventricle (~23 times the frequency of that observed in uninjured ventricles; data not shown) makes it unlikely that they arose from rapid expansion of an existing population of poorly differentiated

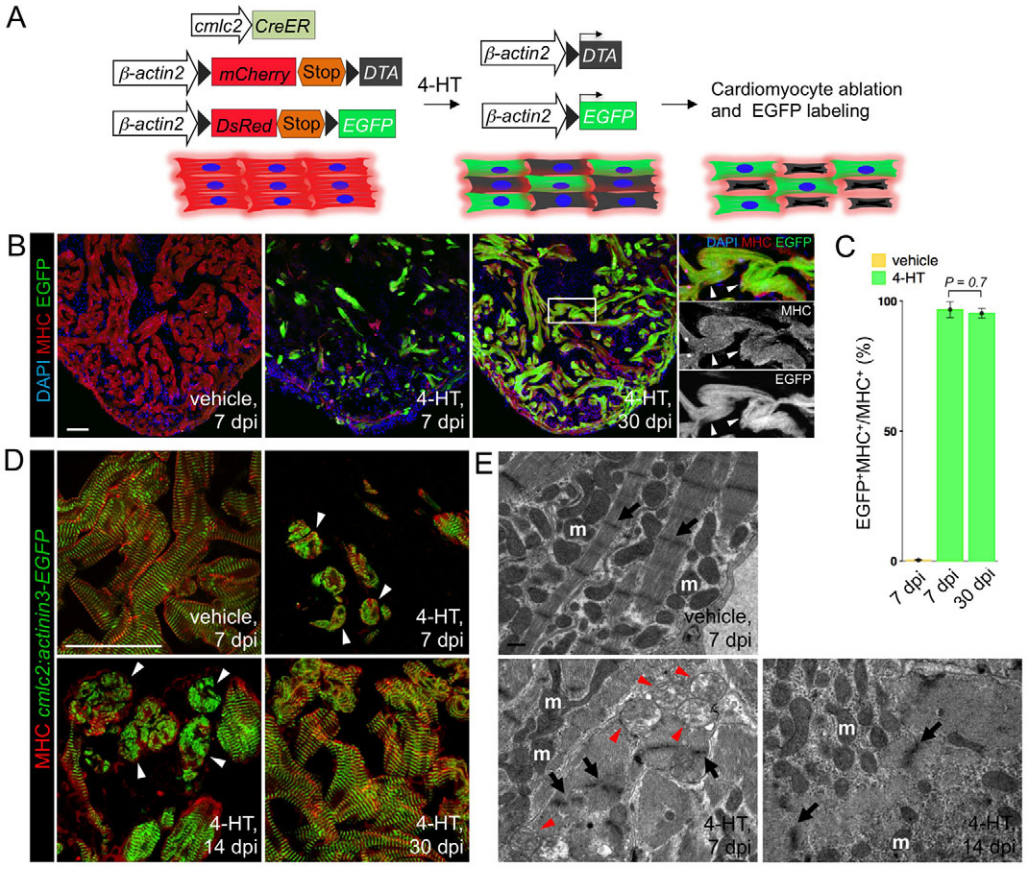

Fig. 6. Lineage-tracing and ultrastructural analysis of regenerating muscle. (**A**) Schematic representation of transgenes used for myocyte ablation and lineage tracing. (**B**) Triple transgenic (Z-CAT; *bactin2:loxp-DsRed-STOP-loxp-EGFP*) zebrafish were injected once with vehicle (left) or 4-HT. In 4-HT-injected animals, EGFP labeled the majority of spared cardiomyocytes by 7 dpi (middle) and the majority of regenerated cardiomyocytes by 30 days post-injection (dpi; right). Arrowheads indicate examples of MHC$^+$ tissue expressing EGFP. (**C**) Quantification of EGFP$^+$ myocardium as a percentage of MHC$^+$ ventricular tissue. At 7 dpi, 96% of myocardium was EGFP-labeled, and 95% at 30 dpi. For each group, 4-10 animals were assessed. Insets show enlarged views of the boxed area. (**D**) Assessment of sarcomere structure in Z-CAT fish crossed to a transgenic strain that labels Z-lines (green). Cardiomyocytes of control animals show well-organized sarcomeres with clear Z-lines. By contrast, many myocytes of 4-HT-injected animals display disorganized sarcomeres and loss of Z-lines (arrowheads) by 7 dpi and 14 dpi. By 30 dpi, sarcomeric structure and Z-lines are typically restored. Scale bars: 50 μm. (**E**) Transmission electron micrographs of ventricular myocytes from vehicle- or 4-HT-injected Z-CAT animals. Control myocytes have prominent sarcomeric structure and normal mitochondria (m), whereas 7 and 14 dpi myocytes appear less organized with fewer Z-lines (arrows) and swollen mitochondria (arrowheads). Scale bar: 0.5 μm.

myocytes. By 30 dpi, sarcomere structure was similar to uninjured ventricles (Fig. 6D). Thus, our results indicate that regenerating cardiomyocytes are primarily derived from spared, mature cardiomyocytes that transiently de-differentiate throughout the ventricle after ablation injury.

Finally, we examined whether cardiomyocytes show electrophysiological evidence of reduced differentiation during regeneration. Optical mapping of action potentials in ventricles from 4-HT-injected Z-CAT fish at 7 dpi revealed a sharp increase in the density of isochrones across the entire myocardium, indicating a slowing of conduction (Fig. 7A,D). This slowing was accompanied by fractionation of the depolarization wavefront, with areas of patchy surface breakthrough that were rarely observed in control hearts. In addition, we observed significant prolongation of action potential duration in the hearts of 4-HT-injected animals at 7 dpi, as well as substantial slowing of action potential upstroke velocities (Fig. 7B,C,E). The conduction slowing and wavefront fractionation observed at 7 dpi suggests markedly reduced coupling between myocytes throughout the regenerating myocardium. The wavefront fractionation might also represent intercalation of non-coupled epicardial cells into the myocardium with resultant conduction block and delayed subepicardial impulse propagation. In addition to the conduction findings, the prolongation of action potential duration and diminution of peak action potential upstroke velocities recapitulate the electrical phenotypes of less differentiated cardiomyocytes (Milan et al., 2009; Panakova et al., 2010). Such changes in action potential upstroke velocity probably represent an increased dependence of depolarization on calcium channel conductance and a reduced role for sodium channel conductance (Chopra et al., 2010; Milan et al., 2009; Panakova et al., 2010). Global myocardial surface conduction progressed towards normal velocities at 14 dpi and 30 dpi, with recovery observed at 45 dpi. Similarly, wavefront fractionation was considerably reduced at 14 dpi and 30 dpi, and had nearly resolved by 45 dpi (Fig. 7A,D). Taken together, these observations indicate that functional de-differentiation and partial uncoupling occur in myocytes regenerating after ablation-induced injury, followed by ultrastructural and electrical recovery.

DISCUSSION

Here, we introduced a model of cardiac injury in zebrafish that facilitates ablation of a high proportion of adult cardiac myocytes. We found that zebrafish survive after depletion of >60% of their ventricular myocardium, but exhibit signs that they are experiencing cardiac failure. In this condition, the cardiac chambers presented as dilated, engorged sacs, that were sparsely muscularized and structurally buoyed by epicardium and endocardium. Despite the extreme effects of these injuries, cardiomyocyte proliferation was robustly initiated and muscle regeneration was rapidly completed. Because this injury model stimulated regenerative events throughout the heart, transient changes in cardiomyocyte sarcomere organization and electrophysiology were clear and widespread, each observation being indicative of de-differentiation. Most impressively, all signs of cardiac failure were reversed concomitantly with these regenerative events. Although observed in a non-mammalian model system, we suggest that these findings provide strong support to the concept of regenerative therapy for certain forms of human heart failure.

Our study reveals other important features of cardiac regenerative capacity. First, it is clear that large areas of internal, destroyed myocardium can be effectively replaced with new cardiomyocytes. Thus, regeneration is not purely a characteristic of cardiomyocytes with greater access to components of a blood clot or that are not encased within spared muscle. As injury is widespread in the cardiac chambers of Z-CAT animals, there is greater participation in regeneration by the inner trabecular form of cardiac muscle than after a ventricular resection injury, illuminating

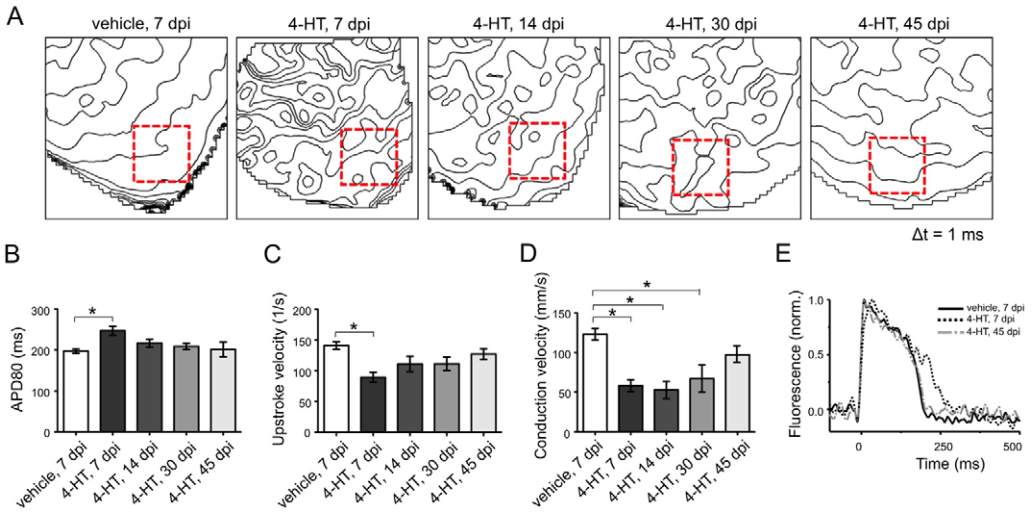

Fig. 7. Electrical properties of ventricular cardiomyocytes after widespread ablation. (**A**) Isochronal maps of ventricular apices from vehicle- or 4-HT-injected Z-CAT fish at indicated time points display the position of the action potential wavefront at 1 ms intervals (Δt=1 ms). Squares show regions of interest (ROIs; 156×156 μm) for epicardial surface conduction velocity estimation shown in D. (**B**,**C**) Action potential duration estimated from 20% depolarization to 80% repolarization (APD_{80}) (B), and derived maximum upstroke velocities (C). Mean±s.e.m. *P<0.05, at 7 dpi and non-significant (NS) at 14, 30 and 45 dpi; one-way ANOVA with Tukey's HSD for comparisons with ventricles from vehicle-injected fish. (**D**) Mean estimated surface myocardium conduction velocities from ROIs in A. Mean±s.e.m. *P<0.05 at 7, 14 and 30 dpi and NS at 45 dpi; one-way ANOVA with Tukey's HSD for comparisons with ventricles from vehicle-injected fish. (**E**) Representative traces of surface action potentials, indicating a slowing of the maximum depolarization rate and an increase in action potential duration at 7 dpi, and their recovery at 45 dpi.

high regenerative potential in this tissue. Our results here also demonstrate for the first time that atrial myocardium is highly regenerative in zebrafish. Second, our results indicate that cardiomyocyte death on its own, as opposed to signals emanating from sheared tissue or a blood clot, is a potent signal for regeneration. How myocyte death instructs regeneration will be an important topic for further investigations. Finally, our data indicate that regeneration occurs with two- to fourfold higher cardiomyocyte proliferation indices after ablation than after resection, an unexpected boost in regenerative efficiency that we suspect reflects structural, vascularizing and/or paracrine influences of non-muscle cells. Whereas cardiomyocyte ablation injury spares and enhances endocardial and epicardial tissues, respectively, a ventricular apex injured by resection, with all major cell types lost in the resected portion, requires repair of the endocardial scaffold and recruitment of a new epicardial covering before these tissues can optimally support muscle regeneration. We also find here that cardiomyocyte death is an efficient attractant for macrophages to injured myofibers in the absence of a large clot, recruitment that might be key to regeneration through tissue debris clearance and/or intercellular signaling.

Regeneration in non-mammalian vertebrate model systems has historically been limited by discovery tools. We suggest that Z-CAT has several advantages as a cardiac injury and regeneration system. Ablation injuries are easy to perform and noninvasive, and extensive injuries can be inflicted without affecting animal viability. Certain questions can also be addressed more sensitively; for example, how cardiomyocyte death triggers developmental responses, such as *raldh2* induction, in epicardial and endocardial tissue. Finally, this system, like nitroreductase ablation systems previously described for larval zebrafish regeneration studies (Curado et al., 2007; Pisharath et al., 2007), has high potential for use in screens to identify new regulators of regeneration. Many adult animals with major cardiac injuries can be generated daily by 4-HT injection or incubation, and the impact of small molecule compounds, mutations or gene manipulations could potentially be assessed in a straightforward manner. Thus, we expect that the ablation/regeneration system described here will enhance efforts to understand how and why heart regeneration occurs in zebrafish. This information, in turn, can inform approaches to muscularizing bioengineered scaffolds, or to reversing ischemic or non-ischemic muscle loss in mammals through regeneration.

Acknowledgements

We thank R. Anderson and D. Stainier for transgenic animals; A. Eastes and P. Williams for zebrafish care; X. Meng (Abmart) and the Developmental Studies Hybridoma Bank for antibodies; M. Gignac for help with electron microscopy; R. Karra for comments on the manuscript; Y. Fang and G. Nachtrab for help with expression analysis; and J. Mably, S. Jin, G. Felsenfeld and A. Nechiporuk, for plasmids. This work was supported by fellowships from AHA (J.W., M.G. and K.K.) and JSPS (K.K.); an AHA Established Investigator Award (0940041N) to D.Y.; grants from NIGMS (GM075846) and March of Dimes to C.A.M.; and grants from American Federation for Aging Research, NHLBI (HL081674), AHA and Pew Charitable Trusts to K.D.P. K.D.P. is an Early Career Scientist for HHMI. Deposited in PMC for release after 6 months.

Competing interests statement

The authors declare no competing financial interests.

Supplementary material

Supplementary material for this article is available at
http://dev.biologists.org/lookup/suppl/doi:10.1242/dev.068601/-/DC1

References

Akazawa, H., Komazaki, S., Shimomura, H., Terasaki, F., Zou, Y., Takano, H., Nagai, T. and Komuro, I. (2004). Diphtheria toxin-induced autophagic cardiomyocyte death plays a pathogenic role in mouse model of heart failure. *J. Biol. Chem.* **279**, 41095-41103.

Beltrami, A. P., Barlucchi, L., Torella, D., Baker, M., Limana, F., Chimenti, S., Kasahara, H., Rota, M., Musso, E., Urbanek, K. et al. (2003). Adult cardiac stem cells are multipotent and support myocardial regeneration. *Cell* **114**, 763-776.

Beltrami, C. A., Finato, N., Rocco, M., Feruglio, G. A., Puricelli, C., Cigola, E., Quaini, F., Sonnenblick, E. H., Olivetti, G. and Anversa, P. (1994). Structural basis of end-stage failure in ischemic cardiomyopathy in humans. *Circulation* **89**, 151-163.

Bersell, K., Arab, S., Haring, B. and Kuhn, B. (2009). Neuregulin1/ErbB4 signaling induces cardiomyocyte proliferation and repair of heart injury. *Cell* **138**, 257-270.

Braunwald, E. and Bonow, R. O. (2010). *Braunwald's Heart Disease: A Textbook of Cardiovascular Medicine*. Philadelphia: Saunders.

Breitman, M. L., Clapoff, S., Rossant, J., Tsui, L. C., Glode, L. M., Maxwell, I. H. and Bernstein, A. (1987). Genetic ablation: targeted expression of a toxin gene causes microphthalmia in transgenic mice. *Science* **238**, 1563-1565.

Brockschnieder, D., Lappe-Siefke, C., Goebbels, S., Boesl, M. R., Nave, K. A. and Riethmacher, D. (2004). Cell depletion due to diphtheria toxin fragment A after Cre-mediated recombination. *Mol. Cell. Biol.* **24**, 7636-7642.

Chablais, F., Veit, J., Rainer, G. and Jazwinska, A. (2011). The zebrafish heart regenerates after cryoinjury-induced myocardial infarction. *BMC Dev. Biol.* **11**, 21.

Chopra, S. S., Stroud, D. M., Watanabe, H., Bennett, J. S., Burns, C. G., Wells, K. S., Yang, T., Zhong, T. P. and Roden, D. M. (2010). Voltage-gated sodium channels are required for heart development in zebrafish. *Circ. Res.* **106**, 1342-1350.

Curado, S., Anderson, R. M., Jungblut, B., Mumm, J., Schroeter, E. and Stainier, D. Y. (2007). Conditional targeted cell ablation in zebrafish: a new tool for regeneration studies. *Dev. Dyn.* **236**, 1025-1035.

Drenckhahn, J. D., Schwarz, Q. P., Gray, S., Laskowski, A., Kiriazis, H., Ming, Z., Harvey, R. P., Du, X. J., Thorburn, D. R. and Cox, T. C. (2008). Compensatory growth of healthy cardiac cells in the presence of diseased cells restores tissue homeostasis during heart development. *Dev. Cell* **15**, 521-533.

Flink, I. L. (2002). Cell cycle reentry of ventricular and atrial cardiomyocytes and cells within the epicardium following amputation of the ventricular apex in the axolotl, Amblystoma mexicanum: confocal microscopic immunofluorescent image analysis of bromodeoxyuridine-labeled nuclei. *Anat. Embryol.* **205**, 235-244.

Gonzalez-Rosa, J. M., Martin, V., Peralta, M., Torres, M. and Mercader, N. (2011). Extensive scar formation and regression during heart regeneration after cryoinjury in zebrafish. *Development* **138**, 1663-1674.

Ieda, M., Fu, J. D., Delgado-Olguin, P., Vedantham, V., Hayashi, Y., Bruneau, B. G. and Srivastava, D. (2010). Direct reprogramming of fibroblasts into functional cardiomyocytes by defined factors. *Cell* **142**, 375-386.

Jopling, C., Sleep, E., Raya, M., Marti, M., Raya, A. and Belmonte, J. C. (2010). Zebrafish heart regeneration occurs by cardiomyocyte dedifferentiation and proliferation. *Nature* **464**, 606-609.

Kikuchi, K., Holdway, J. E., Werdich, A. A., Anderson, R. M., Fang, Y., Egnaczyk, G. F., Evans, T., Macrae, C. A., Stainier, D. Y. and Poss, K. D. (2010). Primary contribution to zebrafish heart regeneration by gata4(+) cardiomyocytes. *Nature* **464**, 601-605.

Kikuchi, K., Holdway, J. E., Major, R. J., Blum, N., Dahn, R. D., Begemann, G. and Poss, K. D. (2011). Retinoic acid production by endocardium and epicardium is an injury response essential for zebrafish heart regeneration. *Dev. Cell* **20**, 397-404.

Kikuchi, K., Gupta, V., Wang, J., Holway, J. E., Wills, A. A., Fang, Y. and Poss, K. D. (2011). *tcf21*$^{+}$ epicardial cells adopt non-myocardial fates during zebrafish heart development and regeneration. *Development* **138**, 2895-2902.

Kim, J., Wu, Q., Zhang, Y., Wiens, K. M., Huang, Y., Rubin, N., Shimada, H., Handin, R. I., Chao, M. Y., Tuan, T. L. et al. (2010). PDGF signaling is required for epicardial function and blood vessel formation in regenerating zebrafish hearts. *Proc. Natl. Acad. Sci. USA* **107**, 17206-17210.

Laube, F., Heister, M., Scholz, C., Borchardt, T. and Braun, T. (2006). Re-programming of newt cardiomyocytes is induced by tissue regeneration. *J. Cell Sci.* **119**, 4719-4729.

Laugwitz, K. L., Moretti, A., Lam, J., Gruber, P., Chen, Y., Woodard, S., Lin, L. Z., Cai, C. L., Lu, M. M., Reth, M. et al. (2005). Postnatal isl1+ cardioblasts enter fully differentiated cardiomyocyte lineages. *Nature* **433**, 647-653.

Lawson, N. D. and Weinstein, B. M. (2002). In vivo imaging of embryonic vascular development using transgenic zebrafish. *Dev. Biol.* **248**, 307-318.

Lee, P., Morley, G., Huang, Q., Fischer, A., Seiler, S., Horner, J. W., Factor, S., Vaidya, D., Jalife, J. and Fishman, G. I. (1998). Conditional lineage ablation to model human diseases. *Proc. Natl. Acad. Sci. USA* **95**, 11371-11376.

Lee, Y., Grill, S., Sanchez, A., Murphy-Ryan, M. and Poss, K. D. (2005). Fgf signaling instructs position-dependent growth rate during zebrafish fin regeneration. *Development* **132**, 5173-5183.

Lepilina, A., Coon, A. N., Kikuchi, K., Holdway, J. E., Roberts, R. W., Burns, C. G. and Poss, K. D. (2006). A dynamic epicardial injury response supports progenitor cell activity during zebrafish heart regeneration. *Cell* **127**, 607-619.
McMurray, J. J. (2010). Clinical practice. Systolic heart failure. *N. Engl. J. Med.* **362**, 228-238.
Milan, D. J., Kim, A. M., Winterfield, J. R., Jones, I. L., Pfeufer, A., Sanna, S., Arking, D. E., Amsterdam, A. H., Sabeh, K. M., Mably, J. D. et al. (2009). Drug-sensitized zebrafish screen identifies multiple genes, including GINS3, as regulators of myocardial repolarization. *Circulation* **120**, 553-559.
Oberpriller, J. O. and Oberpriller, J. C. (1974). Response of the adult newt ventricle to injury. *J. Exp. Zool.* **187**, 249-253.
Oh, H., Bradfute, S. B., Gallardo, T. D., Nakamura, T., Gaussin, V., Mishina, Y., Pocius, J., Michael, L. H., Behringer, R. R., Garry, D. J. et al. (2003). Cardiac progenitor cells from adult myocardium: homing, differentiation, and fusion after infarction. *Proc. Natl. Acad. Sci. USA* **100**, 12313-12318.
Panakova, D., Werdich, A. A. and Macrae, C. A. (2010). Wnt11 patterns a myocardial electrical gradient through regulation of the L-type Ca(2+) channel. *Nature* **466**, 874-878.
Pfeffer, M. A., Pfeffer, J. M., Fishbein, M. C., Fletcher, P. J., Spadaro, J., Kloner, R. A. and Braunwald, E. (1979). Myocardial infarct size and ventricular function in rats. *Circ. Res.* **44**, 503-512.
Pisharath, H., Rhee, J. M., Swanson, M. A., Leach, S. D. and Parsons, M. J. (2007). Targeted ablation of beta cells in the embryonic zebrafish pancreas using E. coli nitroreductase. *Mech. Dev.* **124**, 218-229.
Porrello, E. R., Mahmoud, A. I., Simpson, E., Hill, J. A., Richardson, J. A., Olson, E. N. and Sadek, H. A. (2011). Transient regenerative potential of the neonatal mouse heart. *Science* **331**, 1078-1080.
Poss, K. D., Wilson, L. G. and Keating, M. T. (2002). Heart regeneration in zebrafish. *Science* **298**, 2188-2190.
Rumyantsev, P. P. (1973). Post-injury DNA synthesis, mitosis and ultrastructural reorganization of adult frog cardiac myocytes. An electron microscopic-autoradiographic study. *Z. Zellforsch. Mikrosk. Anat.* **139**, 431-450.
Saito, M., Iwawaki, T., Taya, C., Yonekawa, H., Noda, M., Inui, Y., Mekada, E., Kimata, Y., Tsuru, A. and Kohno, K. (2001). Diphtheria toxin receptor-mediated conditional and targeted cell ablation in transgenic mice. *Nat. Biotechnol.* **19**, 746-750.
Schnabel, K., Wu, C. C., Kurth, T. and Weidinger, G. (2011). Regeneration of cryoinjury induced necrotic heart lesions in zebrafish is associated with epicardial activation and cardiomyocyte proliferation. *PLoS ONE* **6**, e18503.
Srinivas, S., Watanabe, T., Lin, C. S., William, C. M., Tanabe, Y., Jessell, T. M. and Costantini, F. (2001). Cre reporter strains produced by targeted insertion of EYFP and ECFP into the ROSA26 locus. *BMC Dev. Biol.* **1**, 4.
Stanger, B. Z., Tanaka, A. J. and Melton, D. A. (2007). Organ size is limited by the number of embryonic progenitor cells in the pancreas but not the liver. *Nature* **445**, 886-891.
Tajbakhsh, S. (2009). Skeletal muscle stem cells in developmental versus regenerative myogenesis. *J. Intern. Med.* **266**, 372-389.
Traver, D., Paw, B. H., Poss, K. D., Penberthy, W. T., Lin, S. and Zon, L. I. (2003). Transplantation and in vivo imaging of multilineage engraftment in zebrafish bloodless mutants. *Nat. Immunol.* **4**, 1238-1246.
Wills, A. A., Holdway, J. E., Major, R. J. and Poss, K. D. (2008). Regulated addition of new myocardial and epicardial cells fosters homeostatic cardiac growth and maintenance in adult zebrafish. *Development* **135**, 183-192.
Winter, E. M., Grauss, R. W., Hogers, B., van Tuyn, J., van der Geest, R., Lie-Venema, H., Steijn, R. V., Maas, S., DeRuiter, M. C., deVries, A. A. et al. (2007). Preservation of left ventricular function and attenuation of remodeling after transplantation of human epicardium-derived cells into the infarcted mouse heart. *Circulation* **116**, 917-927.